Dynamical Two-Mode Squeezing of Thermal Fluctuations in a Cavity Optomechanical System

A. Pontin,[1,2] M. Bonaldi,[3,4] A. Borrielli,[3,4] L. Marconi,[1] F. Marino,[2,5] G. Pandraud,[6] G. A. Prodi,[4,7] P. M. Sarro,[6] E. Serra,[4,6] and F. Marin[1,2,5,8,*]

[1]*Dipartimento di Fisica e Astronomia, Università di Firenze, Via Sansone 1, I-50019 Sesto Fiorentino (FI), Italy*
[2]*INFN, Sezione di Firenze, Via Sansone 1, I-50019 Sesto Fiorentino (FI), Italy*
[3]*Institute of Materials for Electronics and Magnetism, Nanoscience-Trento-FBK Division, 38123 Povo, Trento, Italy*
[4]*Istituto Nazionale di Fisica Nucleare (INFN), Trento Institute for Fundamental Physics and Application, I-38123 Povo, Trento, Italy*
[5]*CNR-INO, Largo Enrico Fermi 6, I-50125 Firenze, Italy*
[6]*Department of Microelectronics and Computer Engineering /ECTM/DIMES, Delft University of Technology, Feldmanweg 17, 2628 CT Delft, Netherlands*
[7]*Dipartimento di Fisica, Università di Trento, I-38123 Povo, Trento, Italy*
[8]*European Laboratory for Non-Linear Spectroscopy (LENS), Via Carrara 1, I-50019 Sesto Fiorentino (FI), Italy*

(Received 8 September 2015; published 8 March 2016)

We report the experimental observation of two-mode squeezing in the oscillation quadratures of a thermal micro-oscillator. This effect is obtained by parametric modulation of the optical spring in a cavity optomechanical system. In addition to stationary variance measurements, we describe the dynamic behavior in the regime of pulsed parametric excitation, showing an enhanced squeezing effect surpassing the stationary 3 dB limit. While the present experiment is in the classical regime, our technique can be exploited to produce entangled, macroscopic quantum optomechanical modes.

DOI: 10.1103/PhysRevLett.116.103601

Cavity optomechanics [1] is achieving several major experimental breakthroughs, including the optical cooling of optomechanical oscillators down to a thermal occupation number around or below unity [2–7]. A great deal of attention is now devoted to possible realizations of strongly nonclassical states of macroscopic variables that would open the way to new quantum information tools, as well as to crucial tests on the classical-to-quantum transition. In this framework, several techniques to obtain squeezing of the motion quadratures have been studied [8–13] and demonstrated on thermal oscillators [14–20], including quantum nondemolition measurements with modulated [8,16] and pulsed [11,18] readout and parametric excitation [12,14,15,17,19,20]. Very recent reports describe the quantum squeezing of the motion of a cooled nano-oscillator exploiting the mechanical interaction with a microwave field [21–23]. A different class of macroscopic, strongly nonclassical systems can be obtained by involving more than one optical and/or mechanical mode. In particular, two mechanical modes have been exploited in optomechanical hybridization [24–27] and are the basic ingredients of two-mode mechanical squeezing, which is the subject of this work.

A two-mode mechanical squeezed state is characterized by correlated fluctuations between one quadrature of the first oscillating mode and one of the second mode (as well as between the corresponding conjugate quadratures). In a quantum system, such correlations translate into entanglement between the two oscillators, i.e., the mechanical correspondent of optical "twin beams" generated in optical parametric amplifiers [28]. In a suitable combination of quadratures of the two oscillators, the fluctuations are reduced below their standard quantum level (or, in a classical system, below the thermal noise level). Such a reduction can be obtained by implementing a modulation of the spring constant at the sum of the resonance frequencies of the two oscillators. Experimental demonstrations of fully mechanical two-mode squeezing of thermal fluctuations have been recently reported for nano-oscillators where the parametric modulation is obtained by electromechanic driving, either incorporating a piezoelectric transducer directly into the mechanical elements of a device designed on purpose [29] or taking advantage from an accidental resonance with a mode of the substrate of a membrane oscillator [30]. Here we study two-mode thermal squeezing in a cavity optomechanical system, exploiting parametric modulation of the optical spring. Our method, just based on the fundamental optomechanical interaction, is not limited to our specific oscillator and can be extended to a variety of other cavity optomechanical systems, such as optical cavities with a refractive membrane in the middle [6,7,27,31], whispering gallery cavities [5,24,26,32], zipper cavities [24], or systems exploiting the pair of antisymmetric torsion modes in double- or quad-paddle oscillators [33]. In addition to stationary variance and spectrally resolved measurements, we describe analyses of dynamic behavior in nonstationary conditions, showing an enhanced squeezing effect surpassing the stationary limit determined by the onset of parametric instability.

Our silicon oscillator is made on the 70 μm thick device layer of a SOI wafer [34] and is composed of a central mass supported by structured beams [35], balanced by four

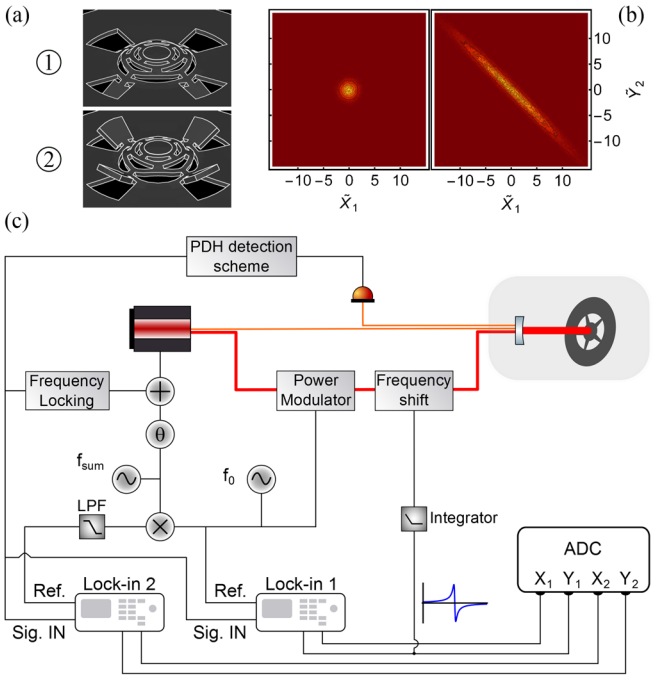

FIG. 1. (a) Shape of the two oscillation modes, obtained by finite elements model simulations. (b) Probability distributions in the $(\tilde{X}_1, \tilde{Y}_2)$ quadratures plane. Left: Thermal distributions, without parametric excitation. Right: With parametric excitation, the fluctuations in the two quadratures are strongly correlated. $\tilde{X}_1$ and $\tilde{Y}_2$ are normalized quadratures of two modes. (c) Experimental setup. The first oscillation mode is parametrically locked at f_0 using the optical spring, as described in Refs. [19,38]. The frequency $f_{\rm sum} - f_0$, corresponding to the resonance of the second mode, is selected after a mixer by the low-pass filter (LPF) and used as reference for the second lock-in amplifier. PDH: Pound-Drever-Hall.

counterweights on the beams' joints [36]. On the surface of the central disk, a multilayer SiO_2/Ta_2O_5 dielectric coating forms a high reflectivity mirror. For the main oscillator mode, labeled 1 in Fig. 1(a) (resonance frequency 172 kHz, effective mass 250 μg), the motion of the mirror is balanced by the motion of the counterweights. As a result, the total recoil on the inner frame is null and the joints become nodal points. In a second oscillation mode, the counterweights move in the same direction of the mirror [mode 2 in Fig. 1(a)], giving slightly different frequency (215 kHz) and mass (100 μg). Thanks to the overall design strategy, both modes reproducibly display a mechanical quality factor of about $Q \simeq 5 \times 10^4$ at room temperature, only limited by the thermoelastic dissipation in the substrate, and the balanced mode exhibits a Q exceeding 10^6 at cryogenic temperature [37]. The oscillator reflecting surface is the end mirror of a $L_{\rm cav} = 1.27$ mm long, high finesse ($\mathcal{F} = 18000$, half-linewidth $\kappa/2\pi = 3.2$ MHz), overcoupled (input mirror transmission $\mathcal{T} = 300$ ppm) Fabry-Perot cavity.

In our setup [Fig. 1(c)], two laser beams derived from the same Nd:YAG source are superimposed with orthogonal polarizations and coupled to the cavity. The first one is used to obtain a signal proportional to the detuning, with a rf sidebands technique. This signal is used to lock the laser to the cavity resonance, with a bandwidth of about 10 kHz, and to measure the oscillator displacement $x(t)$. Furthermore, it is sent to two double-phase digital lock-in amplifiers whose outputs are acquired for the reconstruction of the motion of the oscillating modes. The second, more powerful beam, with a controllable frequency shift with respect to the previous one, sets and controls the optical spring.

The intracavity radiation pressure force, depending on the detuning and therefore on the oscillator position, originates a so-called optical spring [1] that modifies the mechanical resonance frequency. Moreover, due to the finite cavity field buildup time, it changes the effective damping of the oscillator motion, resulting in modal optical cooling (cold damping) when the input radiation frequency $\omega_L/2\pi$ is redshifted with respect to a cavity resonance $\omega_c/2\pi$. In the bad cavity limit and for small detuning (i.e., when both the mechanical frequencies and $\Delta = \omega_L - \omega_c$ are well below κ), the optical spring constant can be approximated as $K_{\rm opt} \simeq (4\omega_L P/L_{\rm cav}\kappa^2 c)\Delta$, where P is the intracavity power. In the same conditions, the effective linewidth becomes $\gamma_{\rm eff} = \gamma_m + \gamma_{\rm opt}$, with $\gamma_{\rm opt} \simeq -(2K_{\rm opt}/m\kappa)$ (m is the mass, $\omega_m/2\pi$ the resonance frequency, and γ the linewidth of the free oscillator) [1,39]. In our experiment, performed at room temperature, we typically use a detuning of $\Delta/\kappa \simeq -0.17$. The oscillation modes are optically cooled down to an effective temperature of $\sim$2.5 K, corresponding to a linewidth $\gamma_{\rm eff}/2\pi = 480$ Hz (800 Hz) and a variance of 110 fm^2 (200 fm^2) for the first (second) mode.

We exploit the optical spring to parametrically stabilize the first oscillation mode at the chosen effective mechanical resonance frequency, against the effect of laser fluctuations [19,38]. Such parametric locking is also useful for the second mode, since it stabilizes the effect of the optical spring.

We now consider two oscillation modes, both changing the cavity length, with displacement $x_i(t)$ ($i = 1, 2$), momentum $p_i(t)$, resonance frequency ω_i, mass m_i, and slowly varying quadratures (X_i, Y_i). In our experiment, the laser detuning is modulated at $\omega_1 + \omega_2$ such that $\Delta \to \Delta[1 + \beta\cos(\omega_1 + \omega_2)t]$ (with $\beta \ll 1$). As a consequence, the optical spring constant is also modulated, and the resulting force is $-(x_1 + x_2)K_\beta \cos(\omega_1 + \omega_2)t$, with $K_\beta = K_{\rm opt}\beta$. Writing the modulated force in terms of the quadratures, we derive that its quasiresonant terms are associated to the two-mode squeezing Hamiltonian $H_I = (K_\beta/4)(X_1X_2 - Y_1Y_2)$, which couples the quadrature X_1 with Y_2 and Y_1 with X_2. The Langevin equations governing their motion can be written as $\dot{\mathbf{X}} + \mathbf{A}\mathbf{X} = \boldsymbol{\xi}$, where $\mathbf{X} = (X, Y)$ can be either (X_1, Y_2) or (Y_1, X_2), $\boldsymbol{\xi}$ is the noise source, and the system matrix is

$$\mathbf{A} = \begin{pmatrix} \frac{\gamma_1}{2} & g_1 \\ g_2 & \frac{\gamma_2}{2} \end{pmatrix}, \quad (1)$$

with $g_i = K_\beta/4\omega_i m_i$. In the following we will just present the results for the (X_1, Y_2) quadratures, since in our experiment Y_1 is exploited (and therefore modified) in the parametric stabilization servo loop [38].

Stationary, null-average solutions are stable if the parametric gain $\overline{g}$ is such that $\overline{g} = K_\beta/2\sqrt{\gamma_1\gamma_2 m_1 m_2 \omega_1 \omega_2} < 1$. In this situation, it is interesting to evaluate the peak spectral densities of the quadratures (at $\omega = 0$). Indeed, they are proportional to the variance measured after integration over periods much longer than $1/\gamma$, which is a frequent experimental procedure.

In the simplified case of oscillators with identical susceptibilities (with mass m, resonance frequency ω_0, damping rate γ), the eigenvalues of $\mathbf{A}$ are simplified to $\lambda_\pm = (\gamma/2)(1 \pm \overline{g})$ and the respective eingenvectors are $X_\pm = (X \pm Y)/\sqrt{2}$. On the combined quadrature X_+, the peak spectral density is reduced by a factor of $(1+\overline{g})^2$, while the total variance is reduced by a factor of $(1+\overline{g})$, with a maximum reduction of, respectively, -6 and -3 dB when approaching the instability threshold. The quadrature X_- has maximal fluctuations, with peak spectral density increased by $1/(1-\overline{g})^2$ with respect to its value in the absence of parametric modulation.

In the realistic case of different parameters between the two oscillation modes, to maintain meaningful combined quadratures it is useful to first normalize each quadrature to its standard value, calculated without parametric excitation [the normalized quadratures are $(\tilde{X}, \tilde{Y})$]. The equations of motion remain formally the same [40]. The general combined quadrature is now defined as $X_\theta = \tilde{X}\cos\theta + \tilde{Y}\sin\theta$, with spectral density $S_\theta(\omega)$ and total variance σ_θ^2. Without parametric excitation, we have symmetric distributions with $S_\theta(0) = 1$ for any value of θ, as shown in the left-hand panel of Fig. 1(b). With parametric excitation, the two quadratures corresponding to eigenvectors of $\mathbf{A}$ still maintain a Lorentzian spectrum, with width $\lambda_\pm$. However, differently from the case of identical oscillators, they do not correspond to extrema in the quadrature fluctuations. $S_\theta(0)$ should be minimized with respect to θ to derive the combined quadrature exhibiting the largest squeezing, in correspondence to $\theta_{\min}$. The experimental probability distribution with parametric driving is shown in the right-hand panel of Fig. 1(b). The strong anticorrelated fluctuations in the two quadratures are clearly revealed by the elongated shape of the graph. In a narrow interval of θ, close to $\pi/4$, the fluctuations of X_θ are below the thermal ones.

It is important to remark that the described picture assumes an exact detection phase. In the realistic case of (small) fluctuations $\Delta\theta$ during the measurement time, the measured minimal spectral density is $S_{\min} + \langle(\Delta\theta)^2\rangle S_{\max}$, where $S_{\min} = S_{\theta_{\min}}(0)$ and $S_{\max} = S_{\theta_{\min}+\pi/2}(0)$ (a similar expression holds for the variance). This feature is crucial to describe the experimental results. The expected minimal spectral density now reaches a minimal value before the instability threshold gain, followed by a deterioration of the squeezing.

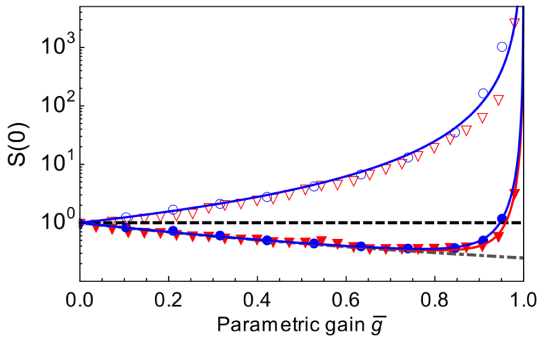

FIG. 2. Experimental measurements of the spectral densities $S_{\min}$ (full symbols) and $S_{\max}$ (empty symbols) as a function of the parametric gain, together with the corresponding theoretical predictions (solid lines). The signals from the four quadratures are preliminarily normalized in order to have unity spectral density in the absence of parametric excitation. Different colors (gray tones) correspond to two data sets, taken with different levels of optical cooling. The lowest measured value of $S_{\min}$ is 0.38 (the theoretical prediction is 0.36). The dash-dotted line shows the prediction for a perfectly stable and optimized detection phase.

In Fig. 2 we show our experimental measurement of $S_{\min}$ and $S_{\max}$ as a function of the parametric gain, together with the corresponding theoretical predictions. The experimental values of $S_{\min}$ and $\theta_{\min}$ are obtained by globally minimizing the peak spectral density of the combined quadrature $(\tilde{X}_1\cos\phi_1 + \tilde{Y}_1\sin\phi_1)\cos\theta + (\tilde{X}_2\sin\phi_2 + \tilde{Y}_2\cos\phi_2)\sin\theta$, with respect to ϕ_1, ϕ_2, and θ, to account for possible errors in the fixed lock-in reference phases.

As expected and already observed [29,30], the squeezing does not surpass -6 dB before the onset of parametric instability. Moreover, $S_{\min}$ reaches a minimum before the instability threshold gain, in contrast to the expected behavior for a perfect and stable detection phase, displayed in Fig. 2 with a gray dash-dotted line. This feature, already observed in recent experiments [29], is well reproduced by the complete model with the parameters of our different oscillating modes. The theoretical values are calculated using independently measured oscillator parameters, and just fitting to the experimental data two parameters: (a) the threshold parametric gain, whose independent estimation is not accurate enough, and (b) the phase variance $\langle(\Delta\theta)^2\rangle$ that results to be around 10^{-3} rad^2.

Above the instability threshold, the system admits no stable solutions and therefore no stationary spectra. However, one can still calculate the behavior of the variance σ^2 in measurements of a quadrature, performed at the time t after the switch-on of the parametric modulation [40].

To start describing the physics involved, we again present the case of identical oscillators. As before, the extrema of the variance are found for $\theta = \pm\pi/4$ at any time t, i.e., in

correspondence to the eigenvectors of $\mathbf{A}$, with $\sigma^2_{\rm min} \equiv \sigma^2_+$ and $\sigma^2_{\rm max} \equiv \sigma^2_-$. The respective temporal evolutions are $\sigma^2_\pm(t) = \sigma^2(0)\{\exp(-2\lambda_\pm t) + (\gamma/2\lambda_\pm)[1-\exp(-2\lambda_\pm t)]\}$. For $\bar{g} > 1$, $\sigma^2_{\rm min}$ approaches $1/(1+\bar{g})$ (i.e., a squeezing exceeding -3 dB) with a time constant $\tau_{\rm short} = 1/2\lambda_+ = 1/\gamma(1+\bar{g})$, while $\sigma^2_{\rm max}$ exponentially diverges with the longer time constant $\tau_{\rm long} = 1/2|\lambda_-| = 1/\gamma(\bar{g}-1)$, exhibiting the critical slowing-down at threshold. If the system dynamic range is large enough, it can be left evolving after the switch-on of the parametric excitation for few $\tau_{\rm short}$, reaching, therefore, a stronger two-mode squeezing with respect to the stationary situation.

For different oscillators, the variances $\sigma_\pm$ in the combined quadratures corresponding to eigenvectors of $\mathbf{A}$ still evolve exponentially with time constants $1/2\lambda_\pm$, while for any other quadrature we expect the combination of exponentials with time constants $1/2\lambda_+$, $1/2\lambda_-$, and $1/(\lambda_+ + \lambda_-)$. As in the stationary case, minimal fluctuations are no longer found for the eigenvector corresponding to λ_+ (except for asymptotically long t, as we will see). Moreover, here the optimal phase θ depends on t, as well as on $\bar{g}$.

We have applied to our system periodic bursts of parametric modulation. The bursts are long enough to observe the system evolution, and are repeated at the rate of 50 Hz. The four output signals of the two lock-in amplifiers (integrated with a time constant of 40 μs) are sampled at $1/\Delta t = 200$ kS/s, then sectioned synchronously with the periodic bursts, so that each section starts at the beginning of a burst. We note that the sampling rate is much larger than $\lambda_\pm$. For each nth data sample, we calculate variances and cross-correlations between the four signals, at the time $n\Delta t$ after the onset of the parametric modulation, over 5000 consecutive bursts. The minimal variance $\sigma^2_{\rm min}$ is obtained by global minimization with respect to the three phases ϕ_1, ϕ_2, and θ. In Fig. 3 we report the time evolution of $\sigma^2_{\rm min}$, together with the prediction of the model, for three levels of gain $\bar{g}$ below, near, and above the instability threshold. As expected, in the last case the variance falls below the stationary limit of ~0.5. The effect of the phase fluctuations $\Delta\theta$ is even more crucial than in stationary conditions. The measurable minimal variance presents a minimum for an optimal value of t, after which it starts increasing due to the mixing with the exploding quadrature. We also remark that, in the absence of phase fluctuations, there is a qualitative difference between the two regimes $\bar{g} < 1$ and $\bar{g} > 1$. In the former case, the minimal variance is always lower than σ^2_+, as in the stationary case (see Fig. 3). Above threshold, instead, it asymptotically converges to σ^2_+, and the combined quadrature with minimal fluctuations tends to coincide with the stable eigenvector.

In conclusion, we have prepared an optomechanical system in a two-mode squeezed thermal state. Some features recently observed in purely mechanical and electromechanical systems, such as the deterioration of the squeezing before the instability threshold, are accurately observed and well reproduced by a model considering different mode parameters. Moreover, we analyze the dynamical evolution after the onset of the parametric modulation and show that the -3 dB limit in the squeezing of the two-mode variance, rigorous in stationary conditions for identical oscillators, is overcome for a bit of time. Even in this case, our model well reproduces the experimental data, and underlines the crucial role of phase fluctuations. Indeed, both the achievable minimal uncertainty and its temporal stability are actually determined by such phase noise.

Our system operates with low optical and mechanical losses and implements optical cooling and frequency control, with a setup similar to those employed to prepare the oscillator close to its ground state. In such conditions, our technique can produce entangled states of the mechanical oscillation modes [41,42]. As shown in Refs. [42,43], the two-mode squeezing variance is an indicator equivalent to the logarithmic negativity, and a value of the combined variance below unity is always a signature of entanglement between the two oscillating modes. For $\bar{g} = 0$, the variance of each quadrature is $(2\bar{n}+1)$, where the occupation

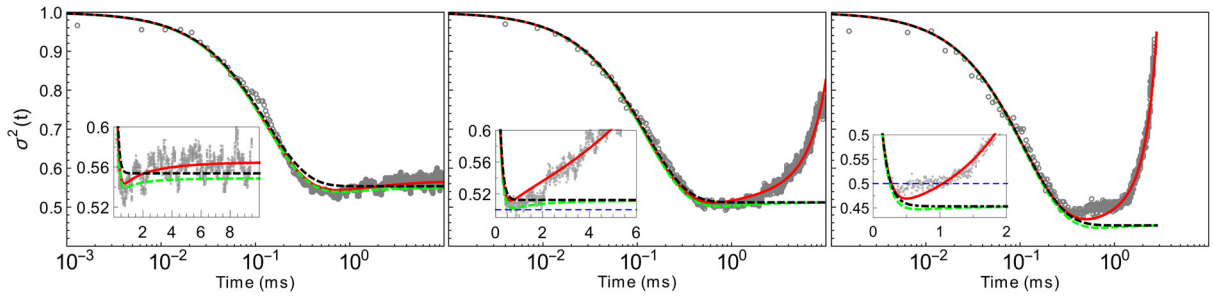

FIG. 3. Time evolution of the experimental minimal variance $\sigma^2_{\rm min}$ after the onset of the parametric modulation (symbols), together with the prediction of the model (solid lines), for different modulation amplitudes. The normalized parametric gains $\bar{g}$ extracted from the fits are (a) $\bar{g} = 0.92$, (b) $\bar{g} = 1.06$, (c) $\bar{g} = 1.30$. The second fit parameter is the phase noise, which results to be (a) $\Delta\theta_{\rm rms} = 0.041$ rad, (b) $\Delta\theta_{\rm rms} = 0.045$ rad, (c) $\Delta\theta_{\rm rms} = 0.070$ rad. The variance is measured over 5000 consecutive bursts, repeated at the rate of 50 Hz. The duty cycle is 50% for (a) and (b) and 15% for (c). Light (green) dashed lines: predicted evolution in the absence of phase noise ($\Delta\theta = 0$). Black dashed lines: predicted evolution of σ^2_+.

number $\overline{n}$ must be calculated using the effective temperature actually achieved by optical cooling. If the variance can be squeezed by a factor of ~ 2, the preliminary requirement is thus a precooling down to $\overline{n} < 0.5$. Our oscillator is relatively heavy (its zero-point motion is as low as 10^{-17} m) and its preparation close to the ground state is still in progress. However, we stress that the methods described in this Letter can be applied, e.g., to systems with SiN refractive membranes that have recently achieved thermal occupation numbers not far from the requirement (e.g., $\overline{n} = 0.84 \pm 0.22$ is reported in Ref. [7]).

Thanks to its flexibility, our method opens the way to more elaborate schemes including more than two oscillating modes, overcoming the experimentally challenging requirement of equal oscillation frequencies, and leading to experimental studies of complex multipartite entanglement in macroscopic systems. The experimental techniques described here can also be applied to different devices embedded in the same optical cavity, or even in separated cavities sharing the same optical field [44], thus producing well-separated, entangled macroscopic oscillators, particularly interesting for investigating quantum decoherence.

This work has been supported by MIUR (PRIN 2010-2011 and QUANTOM project) and by INFN (HUMOR project). A. B. acknowledges support from the MIUR under the "FIRB-Futuro in ricerca" funding program, project code RBFR13QUVI.

*marin@fi.infn.it

[1] M. Aspelmeyer, T. Kippenberg, and F. Marquardt, Rev. Mod. Phys. **86**, 1391 (2014).
[2] A. D. O'Connell *et al.*, Nature (London) **464**, 697 (2010).
[3] J. D. Teufel, T. Donner, D. Li, J. W. Harlow, M. S. Allman, K. Cicak, A. J. Sirois, J. D. Whittaker, K. W. Lehnert, and R. W. Simmonds, Nature (London) **475**, 359 (2011).
[4] J. Chan, T. P. Mayer Alegre, A. H. Safavi-Naeini, J. T. Hill, A. Krause, S. Gröblacher, M. Aspelmeyer, and O. Painter, Nature (London) **478**, 89 (2011).
[5] E. Verhagen, S. Deléglise, S. Weis, A. Schliesser, and T. J. Kippenberg, Nature (London) **482**, 63 (2012).
[6] T. P. Purdy, P.-L. Yu, N. S. Kampel, R. W. Peterson, K. Cicak, R. W. Simmonds, and C. A. Regal, Phys. Rev. A **92**, 031802(R) (2015).
[7] M. Underwood, D. Mason, D. Lee, H. Xu, L. Jiang, A. B. Shkarin, K. Børkje, S. M. Girvin, and J. G. E. Harris, Phys. Rev. A **92**, 061801(R) (2015).
[8] A. A. Clerk, F. Marquardt, and K. Jacobs, New J. Phys. **10**, 095010 (2008).
[9] K. Jähne, C. Genes, K. Hammerer, M. Wallquist, E. S. Polzik, and P. Zoller, Phys. Rev. A **79**, 063819 (2009).
[10] A. Mari and J. Eisert, Phys. Rev. Lett. **103**, 213603 (2009).
[11] M. R. Vanner, Phys. Rev. X **1**, 021011 (2011).
[12] A. Szorkovszky, A. C. Doherty, G. I. Harris, and W. P. Bowen, Phys. Rev. Lett. **107**, 213603 (2011).
[13] M. Asjad, G. S. Agarwal, M. S. Kim, P. Tombesi, G. Di Giuseppe, and D. Vitali, Phys. Rev. A **89**, 023849 (2014).
[14] D. Rugar and P. Grütter, Phys. Rev. Lett. **67**, 699 (1991).
[15] T. Briant, P. F. Cohadon, M. Pinard, and A. Heidmann, Eur. Phys. J. D **22**, 131 (2003).
[16] J. B. Hertzberg, T. Rocheleau, T. Ndukum, M. Savva, A. A. Clerk, and K. C. Schwab, Nat. Phys. **6**, 213 (2010).
[17] A. Szorkovszky, G. A. Brawley, A. C. Doherty, and W. P. Bowen, Phys. Rev. Lett. **110**, 184301 (2013).
[18] M. R. Vanner, J. Hofer, G. D. Cole, and M Aspelmeyer, Nat. Commun. **4**, 2295 (2013).
[19] A. Pontin, M. Bonaldi, A. Borrielli, F. S. Cataliotti, F. Marino, G. A. Prodi, E. Serra, and F. Marin, Phys. Rev. Lett. **112**, 023601 (2014).
[20] M. Poot, K. Y. Fong, and H. X. Tang, Phys. Rev. A **90**, 063809 (2014).
[21] E. E. Wollman, C. U. Lei, A. J. Weinstein, J. Suh, A. Kronwald, F. Marquardt, A. A. Clerk, and K. C. Schwab, Science **349**, 952 (2015).
[22] J.-M. Pirkkalainen, E. Damskägg, M. Brandt, F. Massel, and M. A. Sillanpää, Phys. Rev. Lett. **115**, 243601 (2015).
[23] F. Lecocq, J. B. Clark, R. W. Simmonds, J. Aumentado, and J. D. Teufel, Phys. Rev. X **5**, 041037 (2015).
[24] Q. Lin, J. Rosenberg, D. Chang, R. Camacho, M. Eichenfield, K. J. Vahala, and O. Painter, Nat. Photonics **4**, 236 (2010).
[25] F. Massel, S. U. Cho, J.-M. Pirkkalainen, P. J. Hakonen, T. T. Heikkilä, and M. A. Sillanpää, Nat. Commun. **3**, 987 (2012).
[26] M. Zhang, G. S. Wiederhecker, S. Manipatruni, A. Barnard, P. McEuen, and M. Lipson, Phys. Rev. Lett. **109**, 233906 (2012).
[27] A. B. Shkarin, N. E. Flowers-Jacobs, S. W. Hoch, A. D. Kashkanova, C. Deutsch, J. Reichel, and J. G. E. Harris, Phys. Rev. Lett. **112**, 013602 (2014).
[28] C. Gerry and P. Knight, *Introductory Quantum Optics* (Cambridge University Press, Cambridge, England, 2005).
[29] I. Mahboob, H. Okamoto, K. Onomitsu, and H. Yamaguchi, Phys. Rev. Lett. **113**, 167203 (2014).
[30] Y. S. Patil, S. Chakram, L. Chang, and M. Vengalattore, Phys. Rev. Lett. **115**, 017202 (2015).
[31] A. M. Jayich, J. C. Sankey, B. M. Zwickl, C. Yang, J. D. Thompson, S. M. Girvin, A. A. Clerk, F. Marquardt, and J. G. E. Harris, New J. Phys. **10**, 095008 (2008).
[32] A. Schliesser, G. Anetsberger, R. Rivière, O. Arcizet, and T. J. Kippenberg, New J. Phys. **10**, 095015 (2008).
[33] E. Serra, A. Borrielli, F. S. Cataliotti, F. Marin, F. Marino, A. Pontin, G. A. Prodi, and M. Bonaldi, Phys. Rev. A **86**, 051801(R) (2012).
[34] E. Serra, A. Bagolini, A. Borrielli, M. Boscardin, F. S. Cataliotti, F. Marin, F. Marino, A. Pontin, G. A. Prodi, M. Vannoni, and M. Bonaldi, J. Micromech. Microeng. **23**, 085010 (2013).
[35] E. Serra, A. Borrielli, F. S. Cataliotti, F. Marin, F. Marino, A. Pontin, G. A. Prodi, and M. Bonaldi, Appl. Phys. Lett. **101**, 071101 (2012).
[36] A. Borrielli *et al.*, Microsyst. Technol. **20**, 907 (2014).
[37] A. Borrielli, A. Pontin, F. S. Cataliotti, L. Marconi, F. Marin, F. Marino, G. Pandraud, G. A. Prodi, E. Serra, and M. Bonaldi, Phys. Rev. Applied **3**, 054009 (2015).

[38] A. Pontin, M. Bonaldi, A. Borrielli, F. S. Cataliotti, F. Marino, G. A. Prodi, E. Serra, and F. Marin, Phys. Rev. A **89**, 023848 (2014).
[39] O. Arcizet, P. F. Cohadon, T. Briant, M. Pinard, and A. Heidmann, Nature (London) **444**, 71 (2006).
[40] See Supplemental Material at http://link.aps.org/supplemental/10.1103/PhysRevLett.116.103601 for details of the normalized equations and their solutions.
[41] J. R. Johansson, N. Lambert, I. Mahboob, H. Yamaguchi, and F. Nori, Phys. Rev. B **90**, 174307 (2014).
[42] J. Li, I. Moaddel Haghighi, N. Malossi, S. Zippilli, and D. Vitali, New J. Phys. **17**, 103037 (2015).
[43] S. Zippilli, G. Di Giuseppe, and D. Vitali, New J. Phys. **17**, 043025 (2015).
[44] A Jöckel, A. Faber, T. Kampschulte, M. Korppi, M. T. Rakher, and P. Treutlein, Nat. Nanotechnol. **10**, 55 (2015).